Available online at www.sciencedirect.com
ScienceDirect
Polymer 48 (2007) 5080–5087
polymer
www.elsevier.com/locate/polymer

Strain-induced disorder–order crystalline phase transition in nylon 6 and its miscible blends

V. Miri [a,*], O. Persyn [a], J.M. Lefebvre [a,*], R. Seguela [a], A. Stroeks [b]

[a] *Laboratoire de Structure et Propriétés de l'Etat Solide, UMR CNRS 8008, Université des Sciences et Technologies de Lille, Bât. C6, 59 655 Villeneuve d'Ascq, France*
[b] *DSM Research, P.O. Box 18, 6160 MD Geleen, The Netherlands*

Received 9 March 2007; received in revised form 26 April 2007; accepted 18 June 2007
Available online 23 June 2007

Abstract

This study deals with the structural modifications of a polyamide 6 (PA6) and a miscible blend of this PA6 with an amorphous semi-aromatic copolyamide (PA6/aPA) under tensile drawing. By combining X-ray diffraction and FTIR spectroscopy, the crystalline phase transitions have been investigated as a function of drawing temperature and strain for both systems. A mechanically induced β–α transition has been clearly identified for PA6 at 100 °C and above, whereas the PA6/aPA blend undergoes the same evolution at 130 °C. These threshold temperatures are very close to the upper limit of the glass–rubber transition of the two systems. This is evidence that the amorphous chain mobility plays a major role on the reorganization capability of the crystalline phase towards its stable form. Further discussion is made regarding the physical origin of this phenomenon.

Keywords: Nylon 6; Crystalline phase transitions; Tensile drawing

1. Introduction

Semi-crystalline polymers are complex systems, with an amorphous phase interlaying crystalline lamellae, most of the macromolecular chains being engaged in both phases. Regarding plastic deformation, extensive work has been devoted to the temperature range between the glass transition and the melting point, in which both phases are involved, leading to important changes in crystallographic texture and morphology [1]. Indeed, a gradual lamellar to fibrillar structural transformation has been evidenced for several semi-crystalline polymers under various testing conditions such as uniaxial tension and simple shear experiments [1–3]. Contribution of the amorphous phase has been described in terms of interlamellar slip, interlamellar separation and stack rotation [1,4,5]. Regarding the crystalline phase, the question is addressed according to two rather conflicting approaches. The first one, issued from ''classical'' crystal plasticity considers that plastic flow results from dislocation motions within the lamellae inducing crystallographic slip inside the crystals [6–9]. This model accounts fairly well for experimental results at low strains, such as the yield stress dependence on drawing temperature or lamella thickness [6,7,10,11]. However, this approach cannot explain some observations at large deformations, like the long period change during drawing shown by Peterlin [12,13]. In the latter case, it is assumed that the deformation proceeds by simultaneous melting and recrystallization of the polymer under adiabatic conditions [14–16].

Deformation may induce additional effects on the structure, such as twinning and crystal phase transitions. Twinning, usually observed at small strains, produces a large rotation of the crystallographic lattice around the chain axis due to finite transverse displacement of chains in crystals, while maintaining the original structure. Deformation processes may also be

* Corresponding authors. Tel.: +33 3 20 33 64 16/43 49 55.
E-mail addresses: valerie.miri@univ-lille1.fr (V. Miri), jean-marc.lefebvre@univ-lille1.fr (J.M. Lefebvre).

0032-3861/$ - see front matter © 2007 Elsevier Ltd. All rights reserved.
doi:10.1016/j.polymer.2007.06.039

accompanied by order–disorder, disorder–order and order–order crystal phase transitions that have been investigated in numerous authors [17–26]. In the case of nylon 6, a strain-induced disorder–order reorganization has been clearly identified [27–31]. The mechanism of this phase transformation is still not clearly elucidated. Using atomic force microscopy and Raman microspectroscopy, Ferreiro et al., have shown that for temperatures below 160 °C, plasticity in nylon 6 is governed by the nucleation and propagation of shear bands within the amorphous phase [30,32]. They also found that starting from a spherulitic morphology, the disorder–order transition mainly takes place during the build up of the fibrils. It is therefore of prime importance to determine the role of the amorphous phase in the plastic deformation process. In the case of nylon 6, an interesting opportunity for probing the amorphous phase contribution is afforded by studying nylon 6/amorphous nylon miscible blends as a function of blend composition.

Apart from their potential interest for packaging applications, blends of polyamide 6 (PA6) with an amorphous aromatic copolyamide (aPA) offer a miscible system for which, by varying the aPA content, the crystal weight fraction of the PA6 component may be kept fairly constant while increasing the amorphous content and the glass transition temperature [33].

Initial structure, thermal and mechanical behaviours of PA6/aPA blends have been reported elsewhere [34]. It was shown that the initial morphology is not spherulitic but rather consists of randomly distributed bundles of lamellae. At temperatures above the activation of the amorphous phase relaxation, a ductility improvement has been observed in terms of ultimate drawability upon addition of aPA. This finding has been mainly ascribed to aPA which acts as a diluent of the macromolecular network. Besides, the occurrence of a deformation induced crystal phase transition has been asserted, and the goal of the present paper is to focus on these transitions in PA6/aPA blends and to quantify their evolution as a function of blend composition and temperature by means of X-ray diffraction and FTIR spectroscopy. Probing the role of amorphous phase mobility will be a major issue in this attempt to elucidate the disorder–order crystal phase transformations in PA6.

2. Experimental

2.1. Materials

The aliphatic polyamide 6 supplied by DSM (Akulon F 136) has a weight-average molar mass $M_w = 50$ kDa. The semi-aromatic amorphous polyamide, referred as aPA (Grivory G21 from EMS) is an amorphous copolyamide, PA6I-6T, with isophthalic (I)/terephthalic (T) ratio 0.70/0.30 and $M_w = 8120$ Da.

Pure PA6 and PA6/aPA blend with 60/40 weight ratio were provided by DSM Research. Materials were extruded at 275 °C, cast into films about 80 μm thick on a chill roll at 22 °C and annealed at 100 °C for 5 min. Samples were then stored under vacuum at room temperature prior to stretching. The thermal characterizations of the annealed films have been published elsewhere [30]. The main features are summarised in Table 1.

2.2. Mechanical testing

Dynamic mechanical experiments were performed to evaluate the evolution of the main viscoelastic relaxation with respect to blend composition. Measurements were carried out on a Rheometrics RSA II apparatus operating in tensile mode at a frequency of 1 Hz in the temperature range $0 < T < 180$ °C. Specimens with gauge width and length 7 mm × 22 mm were cut from the cast films.

Tensile tests were performed in the temperature range $70 < T_{draw} < 130$ °C on dried samples. The upper value for the drawing temperature was deliberately chosen to make sure that the observed structural transformations are not thermally induced but originate from plastic straining. Indeed, a previous study has shown that thermally induced crystal transitions significantly occur above 130 °C [33]. Test specimens with 25 mm gauge length and 5 mm width were drawn at a constant crosshead speed of 50 mm/min. For the structural characterization, the local strain, ε, was determined *a posteriori* from the spacing of ink marks printed 1.5 mm apart on the samples prior to deformation.

2.3. Structural characterization

The drawn samples were analyzed in the unloaded state. X-ray diffraction, in combination with infrared spectroscopy, was used to investigate the strain-induced crystal phase changes.

Wide-angle X-ray scattering (WAXS) experiments were carried out at room temperature in transmission mode. The Ni-filtered Cu Kα radiation ($\lambda = 1.54$ Å) was generated by a Phillips tube operated at 40 kV and 20 mA. The 2D X-ray patterns were obtained on flat films, the sample-to-film distance being 90 mm. The X-ray diffraction profiles were recorded on a diffractometer equipped with a curved position-sensitive X-ray multi-detector INEL CPS120. Uniaxially stretched films were fixed on the goniometer so that the draw direction was normal to the detector plane. The diffraction data are thus collected in the equatorial plane in the range $8° < 2\theta < 30°$ with a step interval of about 0.03°. The specific features of the different crystalline structures of PA6 by X-ray diffraction are documented in many papers [27,33,35,36]. The α form is identified by two well-defined reflections at $2\theta = 20°$ and 24°, corresponding to the diffraction of the (200) and

Table 1
Glass transition temperature, T_g, melting point, T_m, crystal weight fraction, W_c, and crystal weight fraction with respect to PA6 only, W_{cPA6}, for pure PA6 and PA6/aPA blend

Material	T_g (°C)	T_m (°C)	W_c (%)	W_{cPA6} (%)
PA6	51	220	27	27
PA6/aPA blend	77	217	15	25

(002) planes, respectively. It can be noticed that the latter corresponds to the H-bond plane. The γ phase exhibits two main diffractions, at $2\theta = 10.5°$ and 21.5°. The mesomorphic β form is characterized by a weak diffraction at about $2\theta = 10°$ and a main diffraction at about $2\theta = 21.5°$, much broader than the one observed for γ phase at about the same scattering angle. The latter feature is relevant to the disordered character of the β phase.

Infrared spectra were collected in transmission mode on the microscope attachment of an FTIR Perkin–Elmer 2000 spectrometer equipped with a narrow range MCT detector. The size of the focused beam on the sample was 100 μm. Each FTIR spectrum consisted of 30 scans recorded over the wave number range 850–1150 cm^{-1} with a resolution of 4 cm^{-1}. The spectrum intensity was normalized with respect to film thickness. Identification of the specific infrared bands for each crystalline form of PA6 as well as for the aPA has been reported in literature [33,37,38]. The absorbance bands at 927, 960 and 1028 cm^{-1} are ascribed to the α form whereas the bands at 914 and 1000 cm^{-1} are assigned to the α form. The absorbance bands at 973 and 1068 cm^{-1} are attributed to both β and α phases. The aPA exhibits a characteristic band at 868 cm^{-1}. These specific bands allow following and quantifying the mechanically induced crystal phase changes in the materials under study. Experimental spectra are considered as the result of a linear combination of "pure component spectra" recorded from PA6 samples having major α, β and γ forms. Every experimental spectrum is fitted by adjusting the proportions of the three pure component spectra [33].

DSC experiments have been carried out on a Perkin–Elmer DSC-7 apparatus. Temperature scale was calibrated using high purity indium and zinc samples. The heating rate was 10 °C/min and the sample weight was about 10 mg.

3. Results

3.1. Mechanical behaviour

Fig. 1 summarises the mechanical relaxation behaviour of PA6 and PA6/aPA homogeneous blend. More details can be found in Ref. [34]. The temperature location of the main relaxation peak is clearly composition dependent due to the higher glass transition temperature of aPA as compared to the amorphous phase of pure PA6. The upper limit of the glass–rubber transition, T_α^{up}, indicated by arrows in Fig. 1 occurs at about 105 °C for PA6 whereas it takes place at about 135 °C for the PA6/aPA blend.

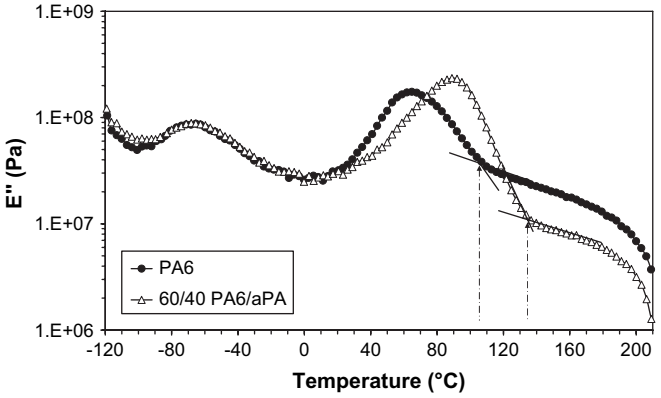

Fig. 1. Loss modulus E'' as a function of temperature for pure PA6 and PA6/aPA blend (dashed arrows indicate upper temperature limit of main relaxation).

Based on these results, the tensile testing experiments were conducted below, above and in the glass–rubber transition range. Pure PA6 was thus tested at 70, 100 and 130 °C, and the blend at 100 and 130 °C. It is worth noticing that whatever be the draw temperature, the two materials exhibit a ductile behaviour [34].

3.2. Structural characterization

Before investigating crystal phase transitions, the crystal content evolution with deformation has been controlled by comparing the melting endotherm of drawn samples with the ones of the isotropic specimens. No significant evolution in melting energy is observed indicating that the crystal content is kept fairly constant with drawing irrespective of blend composition. The DSC thermogram of PA6/aPA blend already reported in the previous mechanical study [34] displays a melting endotherm much similar to that of pure PA6. Moreover, as indicated in Table 1, the PA6 crystal weight fraction in the blend is very close to that measured for pure PA6, i.e. insensitive to the presence of the amorphous copolyamide chains. These findings reveal that only PA6 chains are engaged in the crystalline phase of the blend.

Another point of general concern is that considering the large gap between the draw and melting temperature ranges, strain-induced melting–recrystallization phenomena are unlikely to occur. Only solid state processes should be involved during the deformation of pure PA6 and blend cast films, in agreement with Lin–Argon [9] and Ferreiro–Coulon [32] experimental studies of the plastic behaviour of α form of nylon 6.

Fig. 2 displays the WAXS patterns of the pure PA6 and blend uniaxially stretched at 100 °C for various strains. The undrawn pure PA6 sample (Fig. 2a $\varepsilon = 0$) is mainly in disordered state as revealed by the broad diffraction ring located around $2\theta = 21.5°$. As the strain is increased, the initial pattern changes into two well-defined equatorial diffractions at $2\theta = 20°$ and 24° (Fig. 2a $\varepsilon = 1.0$ and $\varepsilon = 2.2$). These reflections become predominant at the higher strain $\varepsilon = 2.2$. This pattern is indicative of an orientation of the chain axis in the stretching direction, in combination with a strain-induced β–α phase transformation.

The WAXS patterns of the PA6/aPA blend (Fig. 2b) display an initial broad scattering relevant to the β form in addition to some contribution of the two diffraction rings characteristic of the α form. Upon drawing at 100 °C, the main scattering located in the equatorial region (Fig. 2b $\varepsilon = 1.7$ and $\varepsilon = 2.6$) reveals a gradual orientation of the chains in the stretching direction. However, no evidence of disorder–order transformation is observed. It even seems that significant crystalline

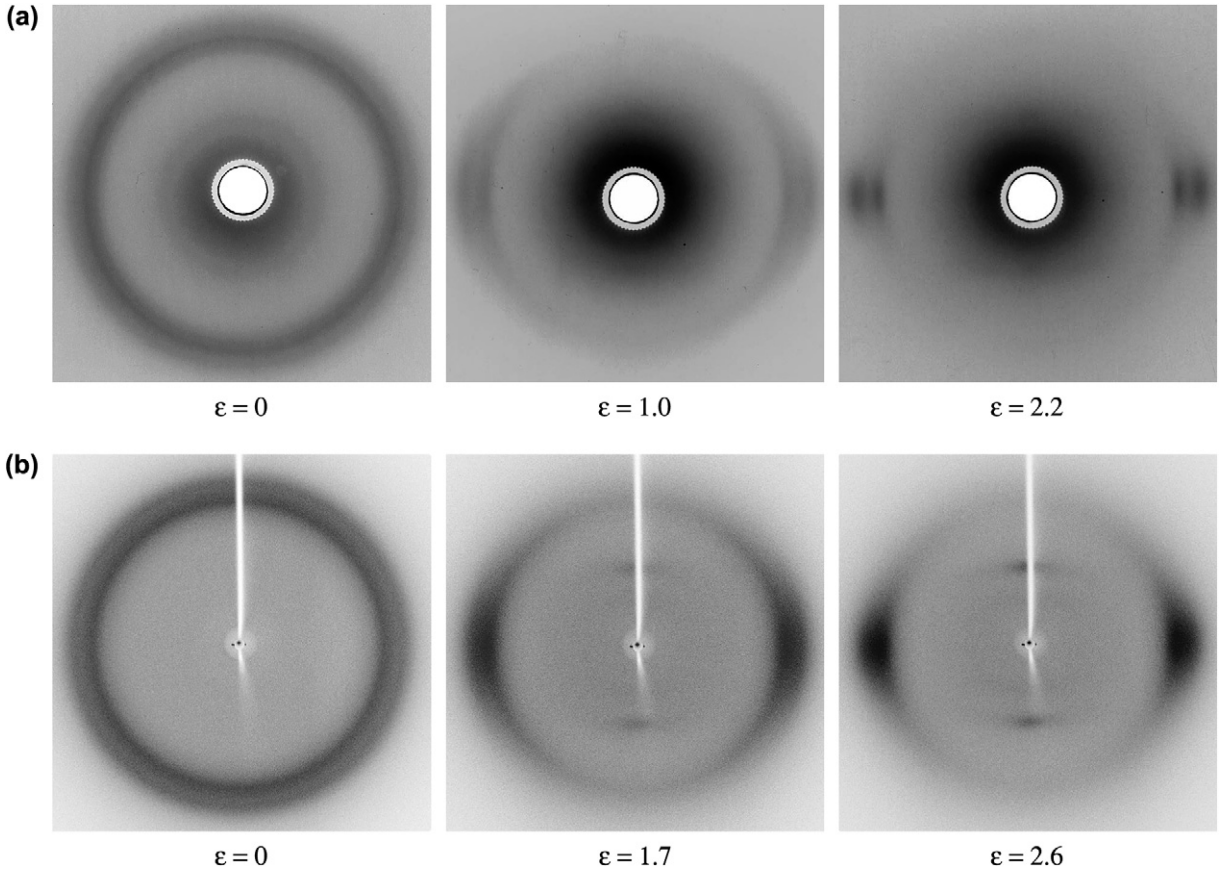

Fig. 2. WAXS patterns of (a) pure PA6 stretched at 100 °C for strains $\varepsilon = 0$, $\varepsilon = 1.0$, $\varepsilon = 2.2$, and (b) the PA6/aPA blend stretched at 100 °C for strains $\varepsilon = 0$, $\varepsilon = 1.7$, and $\varepsilon = 2.6$.

disorder occurs with deformation as judged from the gradual broadening of the equatorial scattering with increasing strain. Besides, the observation of the meridian reflection characteristic of the β phase at about $2\theta = 10°$ corroborates the development of crystalline disorder upon deformation at the expense of the α crystals.

Fig. 3a shows the FTIR spectra of pure PA6 as a function of strain. The characteristic bands of the α phase at 927 and 960 cm^{-1} steadily grow with increasing strain whereas the 973 and 1068 cm^{-1} bands drop. This is clearly indicative of α phase formation upon drawing, in agreement with the previous X-ray observations.

The evolution of the crystalline structure upon drawing for PA6/aPA blend has been also investigated using FTIR spectroscopy. As shown in a previous study [33], the FTIR spectrum of pure aPA exhibits the following valuable features.

- The 868 cm^{-1} band does not interfere with any of the characteristic bands of the various PA6 pure forms: it could therefore be taken as a reference insensitive to strain and phase changes in the PA6 crystalline phase. It also allows checking the aPA content in the blend.
- The lack of aPA band in the wave number range 950–970 cm^{-1} enables monitoring the strain-induced β–α and α–β crystal phase transitions in PA6 without perturbation.

Fig. 3b displays the FTIR spectra recorded at various strains for the PA6/aPA blend stretched at 100 °C. The decrease of the absorbance band at 960 cm^{-1} as the strain is increased reveals a steady drop of α phase content, in perfect support to the previous X-ray observations. Moreover, it can be observed that the absorbance level at 868 cm^{-1} shows no significant evolution with strain, as discussed before.

Based on these FTIR spectra, a quantification of the crystalline phases as a function of strain was achieved by considering a linear combination of the spectra of pure aPA and the so-called pure PA6 components using the same procedure as described in a previous paper [33]. Fig. 4a discloses the results for PA6 stretched at 100 °C as a function of strain. The initial crystalline structure of PA6, mainly the β phase, gradually transforms into α form as the strain is increased. Regarding the bend, the calculated volume fraction of aPA is found to be 40 ± 3%, in very good agreement with the data from blend processing. The relative contribution of each crystalline form in the blend with respect to total PA6 crystal phase content is reported in Fig. 4b as a function of strain. A continuous drop of the α form content is observed as a function of strain, down to the sensitivity limits of the procedure, in parallel with an increased content of the disordered β phase.

Some authors have already reported on a mechanically induced disorder–order transformation in PA6 [27–31]. However, this phenomenon has been barely commented. It is worth

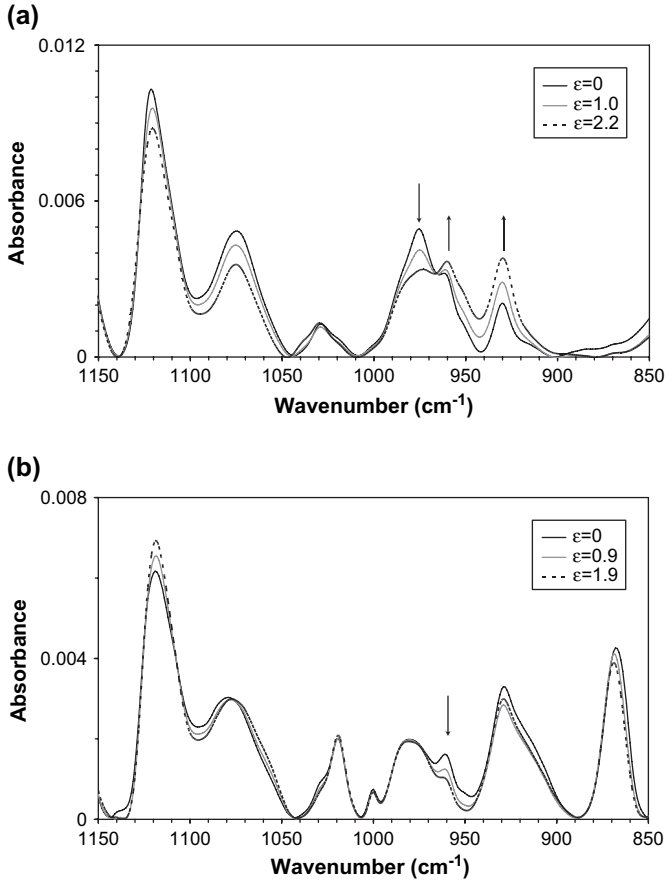

Fig. 3. Infrared spectra of (a) pure PA6 and (b) PA6/aPA blend stretched at 100 °C at various strains.

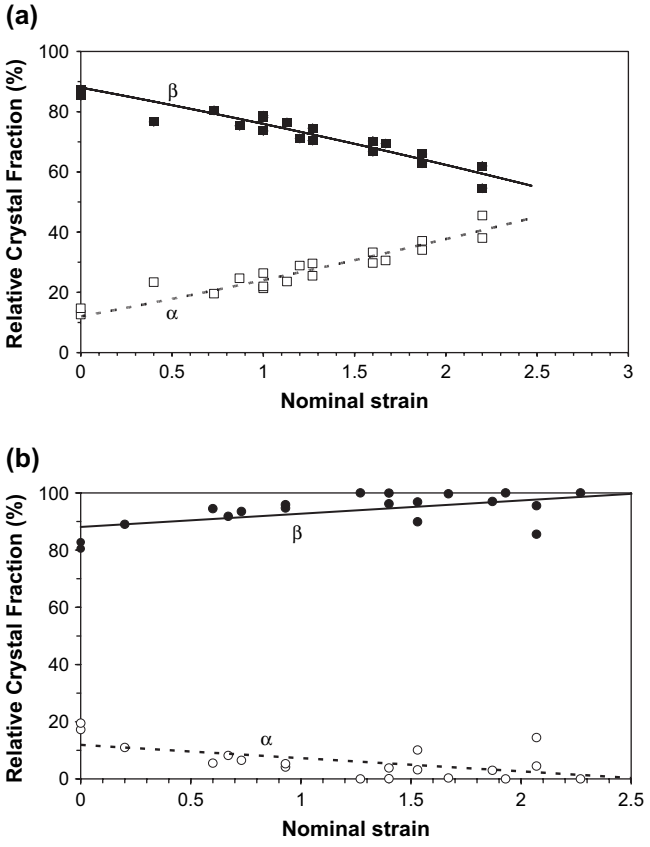

Fig. 4. Evolution of the β and α form relative contents as a function of strain for (a) pure PA6 and (b) PA6/aPA blend drawn at 100 °C.

noticing that the present gradual β−α crystal transition starting at low strains in materials with an initial morphology consisting of bundles of lamella strongly differs from the situation encountered in the case of spherulitic morphology [30]. In the latter case, as mentioned in Section 1, Ferreiro et al., have shown that the β−α transition mainly occurs at high strains during the build up of the fibrils, through the reorientation of the nano-blocks resulting from the lamella fragmentation.

Fig. 5a illustrates the evolution of the FTIR spectra for PA6 drawn up to $\varepsilon = 1.0$ at various draw temperatures. The β−α transformation is clearly favoured at higher draw temperature as indicated by the increase of the 927 and 960 cm^{-1} bands at 130 °C, as compared to the evolution at 100 °C. By contrast, no evidence of disorder−order transition is observed between the isotropic sample and the one stretched at 70 °C. Indeed, the specific bands at 927 and 960 cm^{-1} relative to the α phase even decrease at 70 °C, rather suggesting a reverse trend of increased disorder at this temperature. The quantitative evolution of the crystalline structure upon drawing at 70 and 130 °C reported in Fig. 6 shows that the disorder−order transformation is promoted as the draw temperature is increased. Besides, no significant crystal transition occurs for PA6 stretched at 70 °C till $\varepsilon > 1.8$.

Fig. 7a which depicts the equatorial WAXS scans of PA6 drawn at 70, 100 and 130 °C up to the same strain of $\varepsilon = 2.0$ confirms the above FTIR analysis. In particular, the X-ray profile for PA6 stretched at 70 °C exhibits a broad diffraction peak spanning the scattering range 19−25°, characteristic of β form. Very faint humps close to $2\theta = 21°$ and 23° are relevant to small amount of α crystals, either strain induced or already present in the isotropic film, as suggested by the FTIR data of Fig. 6a. In the latter situation, the appearance of the two faint α form reflections could be due to the disappearance of the γ form reflection at $2\theta = 21.5°$ that masked the presence of the α phase in the isotropic sample. It is worth noticing that the amount of γ crystals in the isotropic film is less than 5%, and therefore undetectable by FTIR.

In contrast to pure PA6, both FTIR and X-ray diffraction revealed an order−disorder transformation for the PA6/aPA blend stretched at 100 °C. Further investigation of the incidence of draw temperature on the phase transition in the blend is reported in Figs. 5b and 7b through the FTIR spectra and X-ray scattering patterns for a strain $\varepsilon = 2.0$. Both kinds of data show that drawing at 130 °C promotes a β−α crystal phase transition contrary to what is observed for samples drawn at 100 °C. Therefore, the PA6/aPA blend behaves at 130 °C in the same way as pure PA6 beyond 100 °C.

4. Discussion

Since the crystalline phase consists of pure PA6 in both PA6 and PA6/aPA blend, one cannot suspect changes in chain mobility in the crystal to be responsible for the different

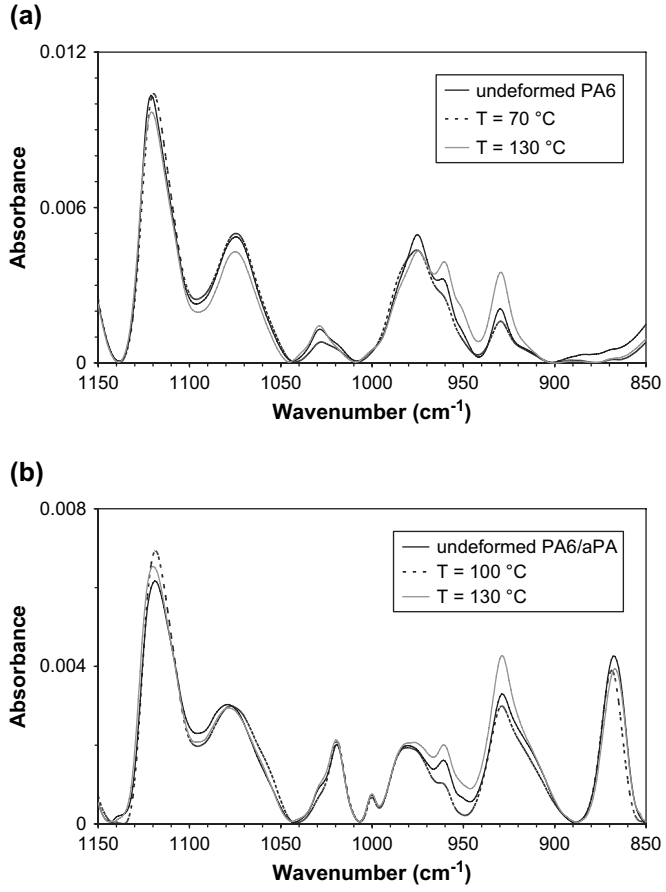

Fig. 5. Infrared spectra of (a) pure PA6 stretched at $\varepsilon = 1.0$ and (b) PA6/aPA blend stretched at $\varepsilon = 2.0$ for different draw temperatures.

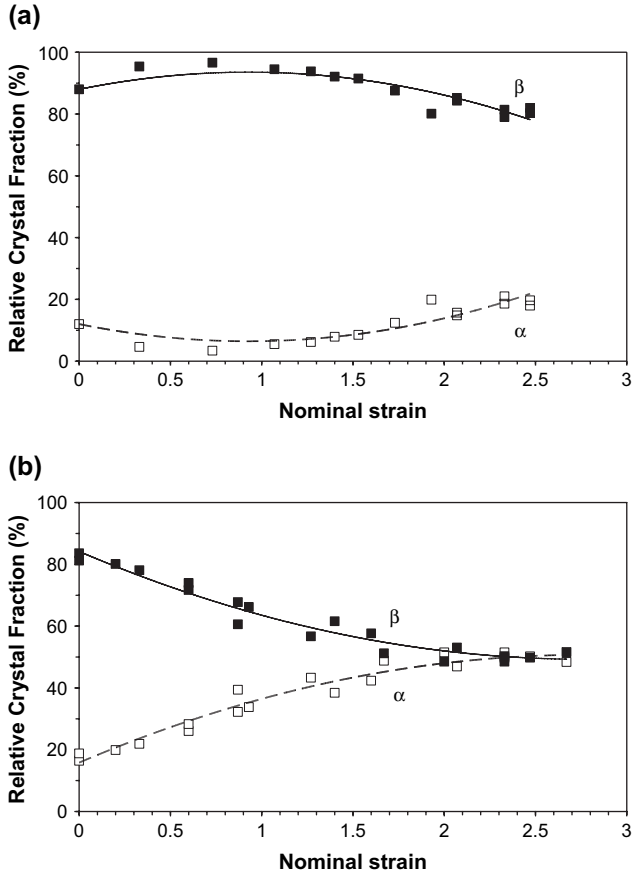

Fig. 6. Evolution of the β and α form relative contents as a function of strain for pure PA6 drawn at (a) $T_{draw} = 70\ ^{\circ}C$ and (b) $T_{draw} = 130\ ^{\circ}C$.

thermal behaviour of the two systems regarding strain-induced phase transitions. Considering that PA6 displays a marked β–α transition at 100 °C and above, whereas the PA6/aPA blend clearly starts to transform at 130 °C, it is worth recalling that there is a 30 °C shift in the temperature location of the main viscoelastic relaxation peak of the blend with respect to that of pure PA6 (Fig. 1). More precisely, these two threshold temperatures for the onset of β–α phase transition correspond to the upper temperature limit, T_{α}^{up}, of the viscoelastic peak associated with the glass–rubber transition for both pure PA6 and the PA6/aPA blend. These features are in favour of suspecting that amorphous chain mobility plays a major role on the reorganization capability of the crystalline phase towards its stable form. For further comparison of PA6 and PA6/aPA blend, Fig. 8 shows the relative crystal content as a function of strain for the two systems drawn at 100 and 130 °C, respectively. Note that in both cases T_{draw} roughly equals T_{α}^{up}. The perfect coincidence of the evolution of the β–α transition in Fig. 8 for both materials points out the key role of the T_{α}^{up} parameter on the strain-induced changes in the crystalline phase. It therefore reinforces the above questioning of a close connection between the reorganization capability of the crystal phase and the chain mobility in the amorphous phase.

Previous studies on strain-induced phase changes in semicrystalline polymers have pointed out the major role of chain mobility in the crystal [18,39]. The situation looks more complex in the present case. First, the fact that the temperature dependence of the crystalline phase transition is different for the pure PA6 and the PA6/aPA blend, whereas the crystalline phase is identical for the two systems, strongly suggests that the phenomenon is governed by factors external to the crystalline phase. Second, since the threshold temperature of the transition is tightly connected with the glass–rubber transition temperature, these external factors are definitely related to the surrounding amorphous phase.

Regarding the chain mobility in the amorphous phase of nylon 6, both the strong dissymmetry of the main relaxation peak associated with molecular mobility in the amorphous phase and the great sensitivity of the high temperature side of this peak to frequency were ascribed to the presence of a so-called constrained amorphous phase [40]. This finding was confirmed by NMR measurements which gave evidence of an amorphous component with reduced mobility above the usual glass transition temperature. It was assigned to a topologically constrained interfacial region [41–43]. The constraints on the amorphous chains due to the anchoring onto the crystal surface, and the dynamic equilibrium of interchain H-bonds in the amorphous phase, even for temperatures far above the glass transition, should be the factors of hindrance of chain mobility in the crystalline phase. More particularly

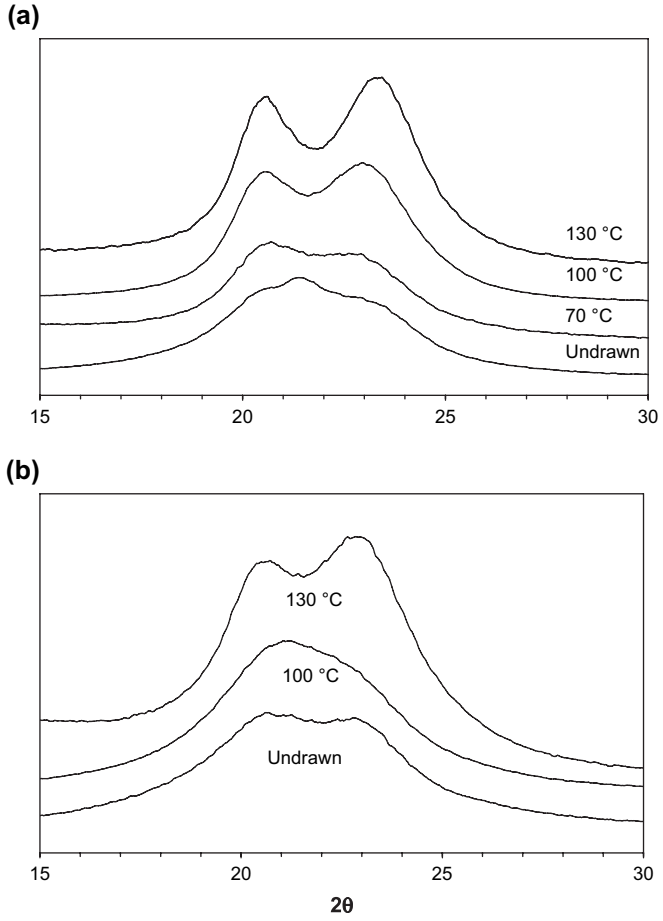

Fig. 7. Equatorial WAXS scans of (a) pure PA6 and (b) PA6/aPA blend drawn at $\varepsilon = 2.0$ for various draw temperatures.

concerned with such hindrance is the translation motion through the crystalline lamella thickness of the crystalline chain stems which need some mobility of the amorphous chain counterpart at the crystal surface. All present experimental findings therefore provide definitive evidence of the intimate dependence of the strain-induced phase change on the complete unlocking of the constrained amorphous phase.

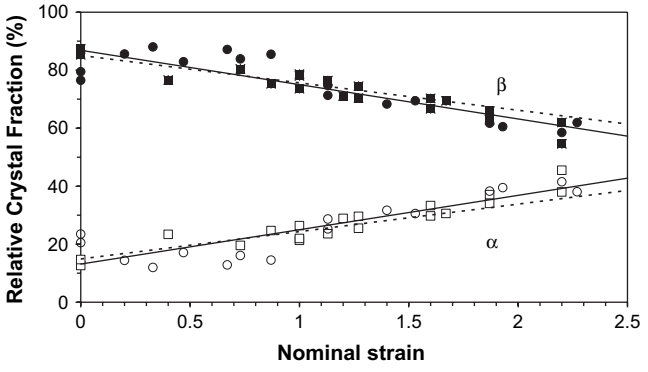

Fig. 8. Comparison of the evolution of the β and α form relative contents for pure PA6 and PA6/aPA blend stretched at $T_{draw} \approx T_{\alpha}^{up}$: □ and ■, pure PA6 for $T_{draw} = 100$ °C; ○ and ●, PA6/aPA for $T_{draw} = 130$ °C.

It is worth adding that the observation of an order–disorder transition for draw temperature below 100 and 130 °C for PA6 and PA6/aPA blend, respectively, is also consistent with the above arguments.

As a final point, we would like to emphasize that the hindrance to the translational motions of the crystalline stems may be the reason why nylon 6 does not display mechanical damping associated with the crystalline phase in spite of the actual activation of libration motions in the crystal.

Acknowledgments

This work was performed with the financial support of DSM Research (Geleen, The Netherland). T. Brink, W. Zoetelief and A. Schmidt from DSM Research are gratefully acknowledged for fruitful discussions.

References

[1] Galeski A. Prog Polym Sci 2003;28:1643–99.
[2] Peterlin A. J Mater Sci 1971;6:490–508.
[3] Schultz J. Polymer materials science. Englewood Cliffs, NJ: Prentice-Hall; 1974.
[4] G'Sell C, Dahoun A. Mater Sci Eng A 1994;175:183–99.
[5] Bartczak Z, Galeski A, Argon AS, Cohen RE. Polymer 1996;37:2113–23.
[6] Young RJ. Philos Mag 1974;30:85–94.
[7] Young RJ. Mater Forum 1988;11:210–6.
[8] Lin L, Argon AS. J Mater Sci 1994;29:294–323.
[9] Lin L, Argon AS. Macromolecules 1994;27:6903–14.
[10] Gaucher-Miri V, Seguela R. Macromolecules 1997;30:1158–67.
[11] Brooks NWJ, Mukhtar M. Polymer 2000;41:1475–80.
[12] Balta-Calleja FJ, Peterlin A, Crist B. J Polym Sci Polym Phys Ed 1972;10(9):1749–56.
[13] Peterlin A. Advances in polymer science and engineering. New York: Plenum Press; 1972. p. 1–19.
[14] Flory PJ, Yoon DY. Nature 1978;272:226–9.
[15] Gent AN, Madan S. J Polym Sci Part B Polym Phys 1989;27:1529–42.
[16] Lucas JC, Failla MD, Smith FL, Mandelkern L, Peacock A. J Polym Eng Sci 1995;35:1117–23.
[17] Saraf R, Porter RS. J Polym Sci Polym Phys Ed 1988;26:1049–57.
[18] Seguela R. J Macromol Sci Part C Polym Rev 2005;45:263–87.
[19] De Rosa C, Auriemma F, De Lucia G, Resconi L. Polymer 2005;9461–75.
[20] Miyasaka K, Makishima K. J Polym Sci 1967;5:3017–27.
[21] Urbanczyk GW. J Polym Sci Polym Symp 1977;58:311–21.
[22] Stepaniak RF, Garton A, Carlsson DJ, Wiles DM. J Appl Polym Sci 1979;23:1747–57.
[23] Murthy NS, Bray RG, Correale ST, Moore RAF. Polymer 1995;36:3863–73.
[24] Vasanthan N, Salem DR. J Polym Sci Part B Polym Phys 2001;39:536–47.
[25] Vasanthan N. J Polym Sci Part B Polym Phys 2003;41:2870–7.
[26] Schreiber R, Veeman WS, Gabriëlse W, Arnauts J. Macromolecules 1999;32:4647–57.
[27] Murthy NS. Polym Commun 1991;32:301–5.
[28] Penel-Pierron L, Seguela R, Lefebvre J-M, Miri V, Depecker C, Jutigny M, et al. J Polym Sci Part B Polym Phys 2001;39:1224–36.
[29] Cole KC, Depecker C, Jutigny M, Lefebvre J-M, Krawczak P. Polym Eng Sci 2004;44:231–40.
[30] Ferreiro V, Depecker C, Laureyns J, Coulon G. Polymer 2004;45:6013–26.

[31] Ziabicki A, Kedzierska K. J Appl Polym Sci 1959;2:14–23.
[32] Ferreiro V, Coulon G. J Polym Sci Part B Polym Phys 2004;42: 687–701.
[33] Persyn O, Miri V, Lefebvre J-M, Depecker C, Gors C, Stroeks A. Polym Eng Sci 2004;44:261–71.
[34] Persyn O, Miri V, Lefebvre J-M, Ferreiro V, Brink T, Stroeks A. J Polym Sci Part B Polym Phys 2006;44:1690–701.
[35] Galeski A, Argon AS, Cohen RE. Macromolecules 1991;3945–52.
[36] Ziabicki A. Kolloid Z 1959;167:132–41.
[37] Rotter G, Ishida H. J Polym Sci 1992;30:489–95.
[38] Umemura J, Murata Y, Tsunashima K, Koizumi N. J Polym Sci Part B Polym Phys 1999;37:531–8.
[39] Penel L, Djezzar K, Lefebvre J-M, Séguéla R, Fontaine H. Polymer 1998;39:4279–87.
[40] Hoashi K, Andrews RD. J Polym Sci Part C 1972;38:387–404.
[41] Mathias LJ, Powell DG, Autran J-P, Porter RS. Mater Sci Eng A 1990; 126:253–63.
[42] Kwak S-Y, Kim JH, Lee J-C. J Polym Sci Part B Polym Phys 2001; 39:993–1000.
[43] Litvinov VM, Penning JP. Macromol Chem Phys 2004;205:1721–34.